Supporting Information

Achieving Efficient Oxygen Reduction on Ultra-Low Metal-Loaded Electrocatalysts by Constructing Well-Dispersed Bimetallic Sites and Interconnected Porous Channels

Chen Deng, [ab‡] Jingjin Tan, [a‡] Cui Ying Toe, [c] Xuan Li, [d] Guodong Li, [b] Xingxing Jiang,[a] Shaomin Wei, [a] Hengpan Yang, [a] Qi Hu [a] and Chuanxin He [a*]

a. Department of Chemistry, College of Chemistry and Environmental Engineering, Shenzhen University, Shenzhen, Guangdong 518060, China.
E-mail: hecx@szu.edu.cn

b. Institute of Microscale Optoelectronics, Shenzhen University, Shenzhen, Guangdong 518060, China.

c. School of Engineering, the University of Newcastle, Callaghan, New South Wales 2308, Australia.

d. Department of Chemical Physics, University of Science and Technology of China, Hefei, Anhui, China

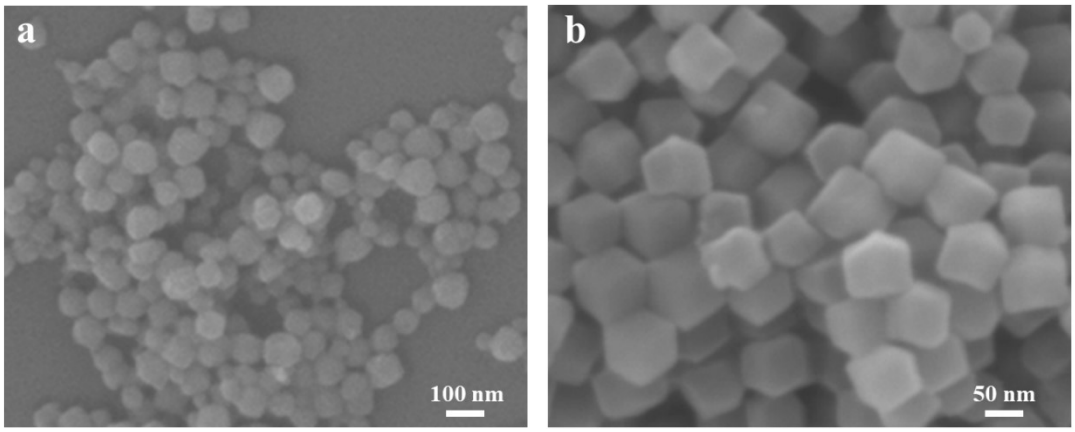

Figure S1. SEM images of ZIF-8 nanoparticles at different magnifications.

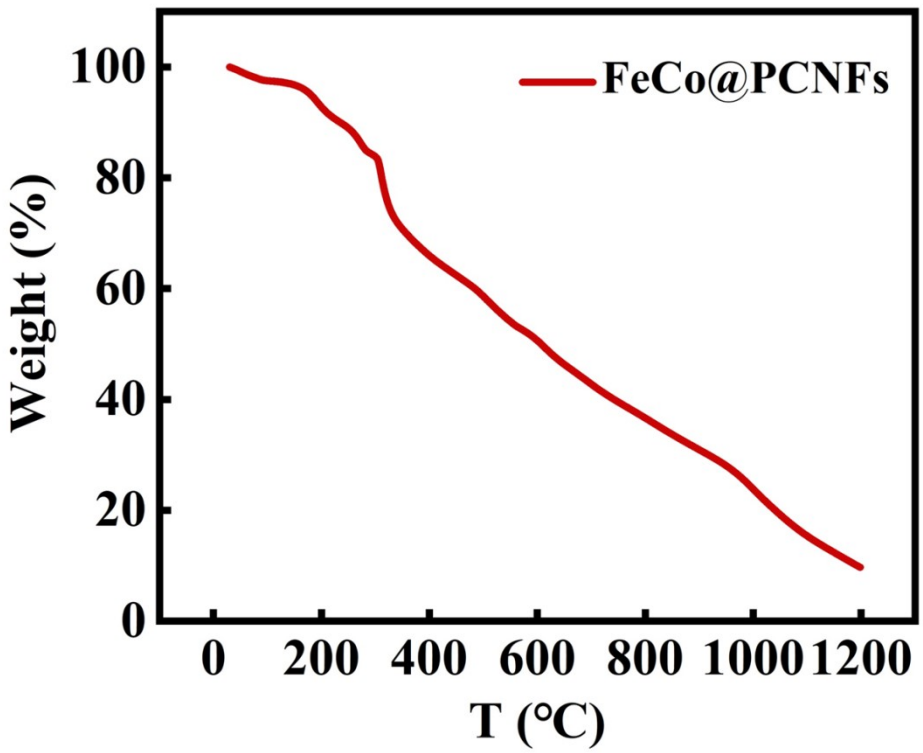

Figure S2. TGA curve of FeCo@PCNFs measured under N_2 atmosphere.

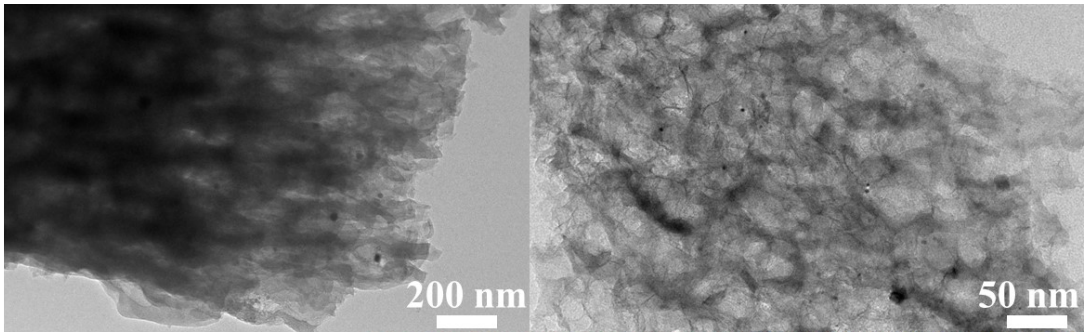

Figure S3. TEM images at high magnification of FeCo@PCNFs.

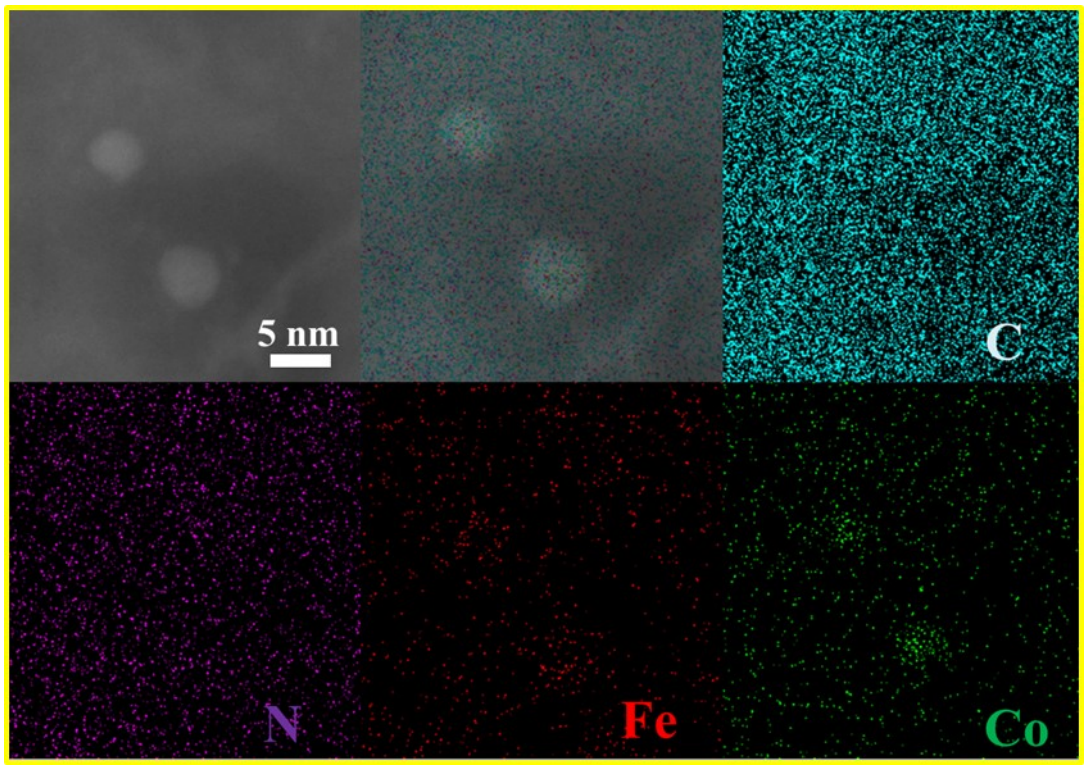

Figure S4. HADDF-STEM-EDX mapping at high magnification of FeCo@PCNFs.

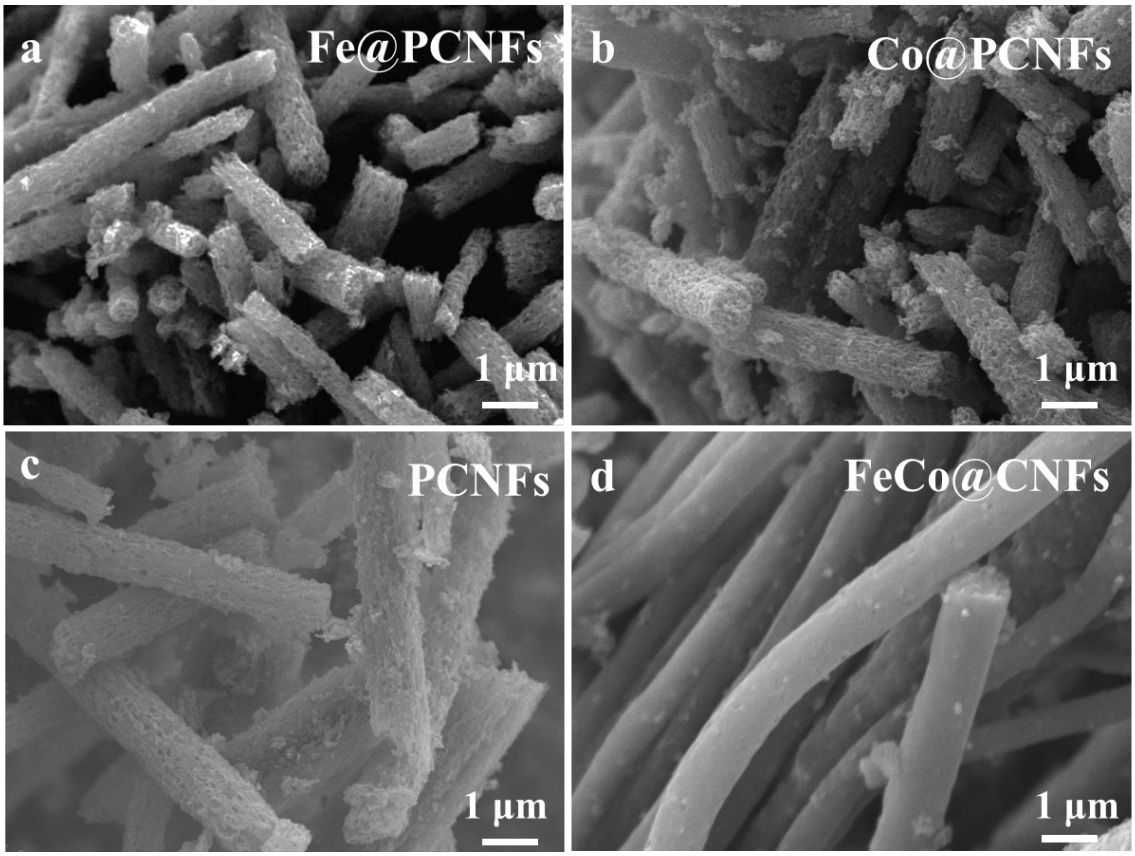

Figure S5 SEM images of all samples: (a) Fe@PCNFs, (b) Co@PCNFs, (c) PCNFs, and (d) FeCo@CNFs.

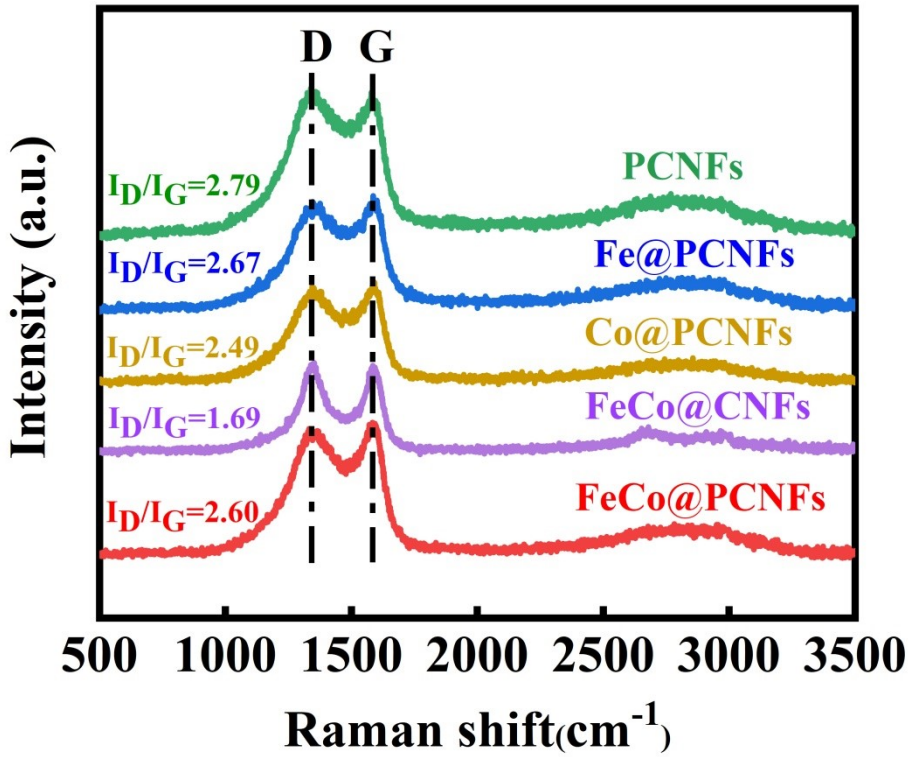

Figure S6. Raman spectra of all samples. I_D/I_G ratios is evaluated by the integral area values of D and G peaks.

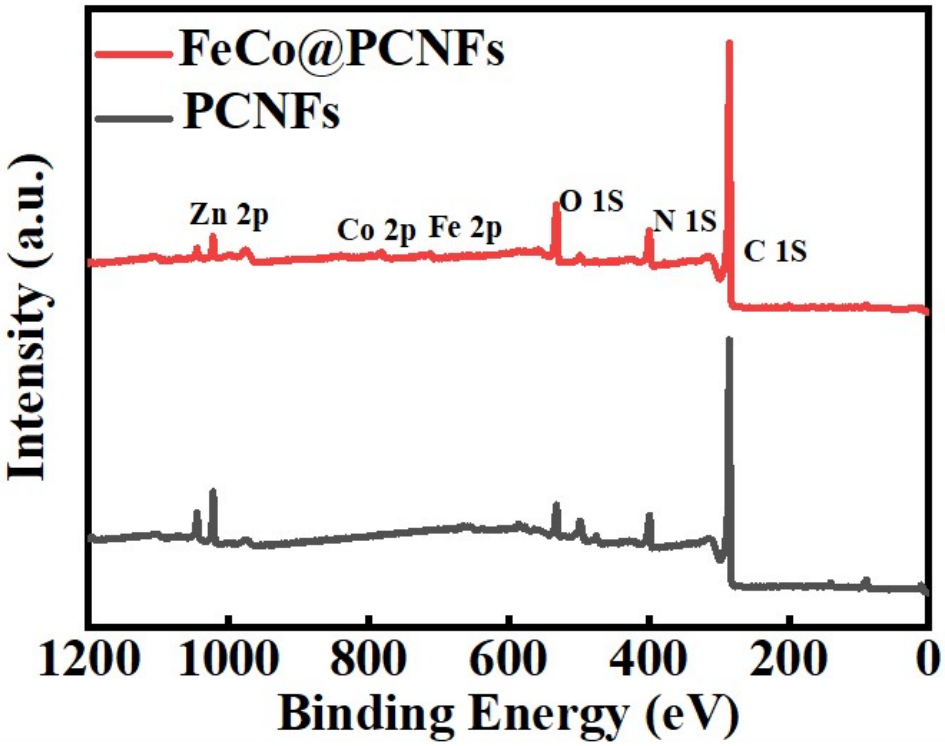

Figure S7. XPS survey spectra of FeCo@PCNFs and PCNFs.

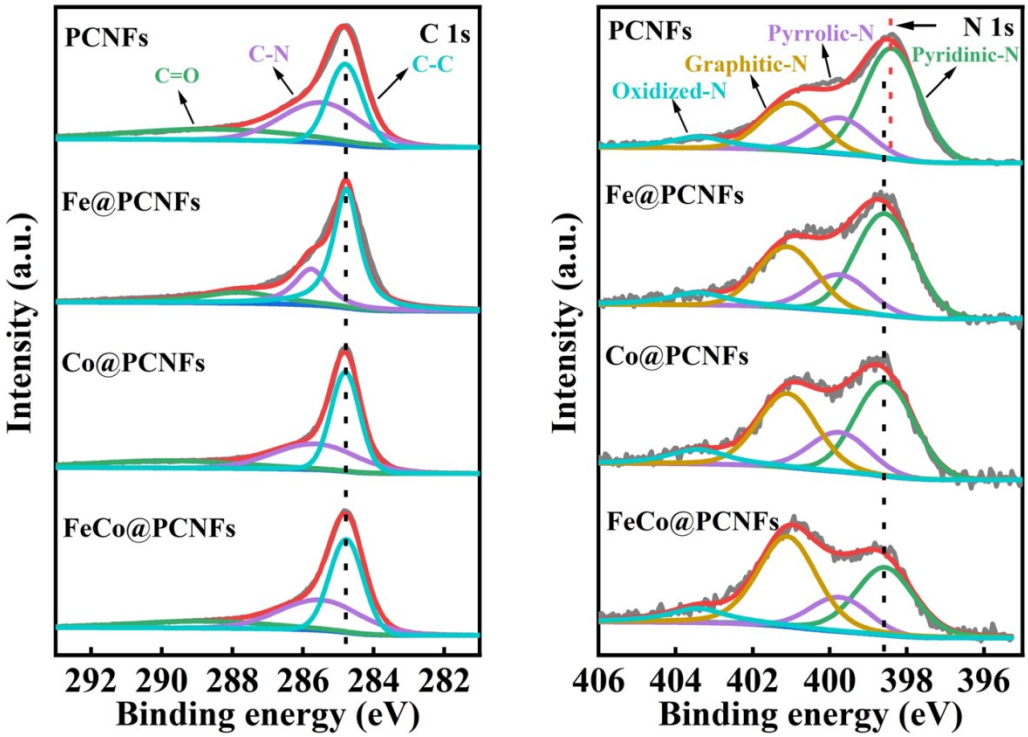

Figure S8. High-resolution XPS spectra of C 1s and N 1s for Fe@PCNFs, Co@PCNFs, FeCo@PCNFs and PCNFs.

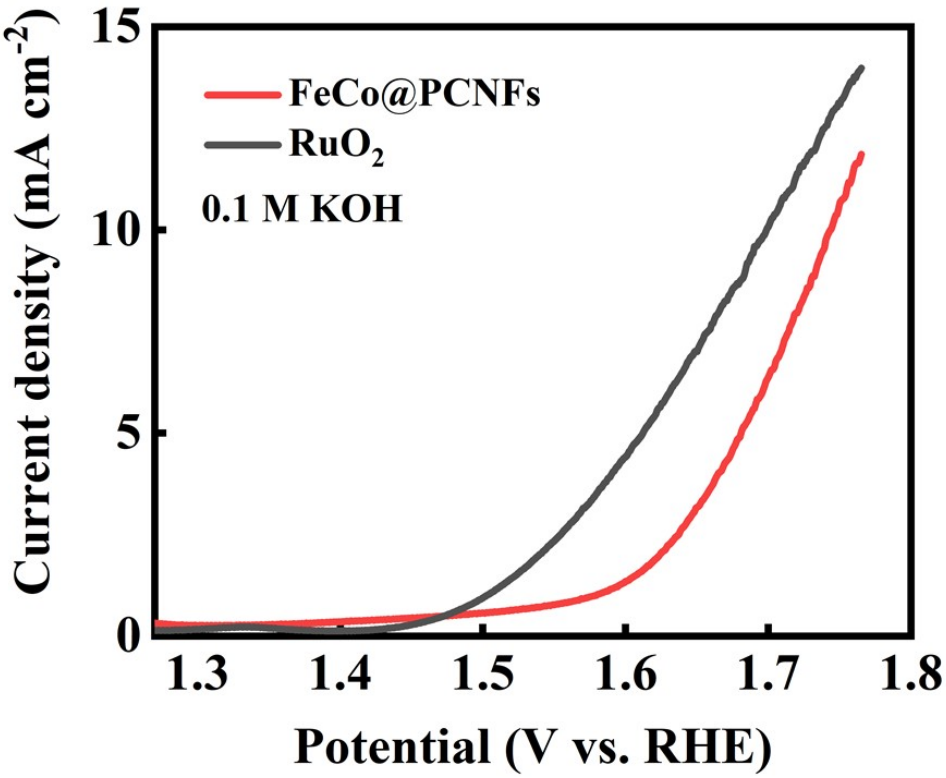

Figure S9. LSV curve of FeCo@PCNFs for the OER in 0.1M KOH solution.

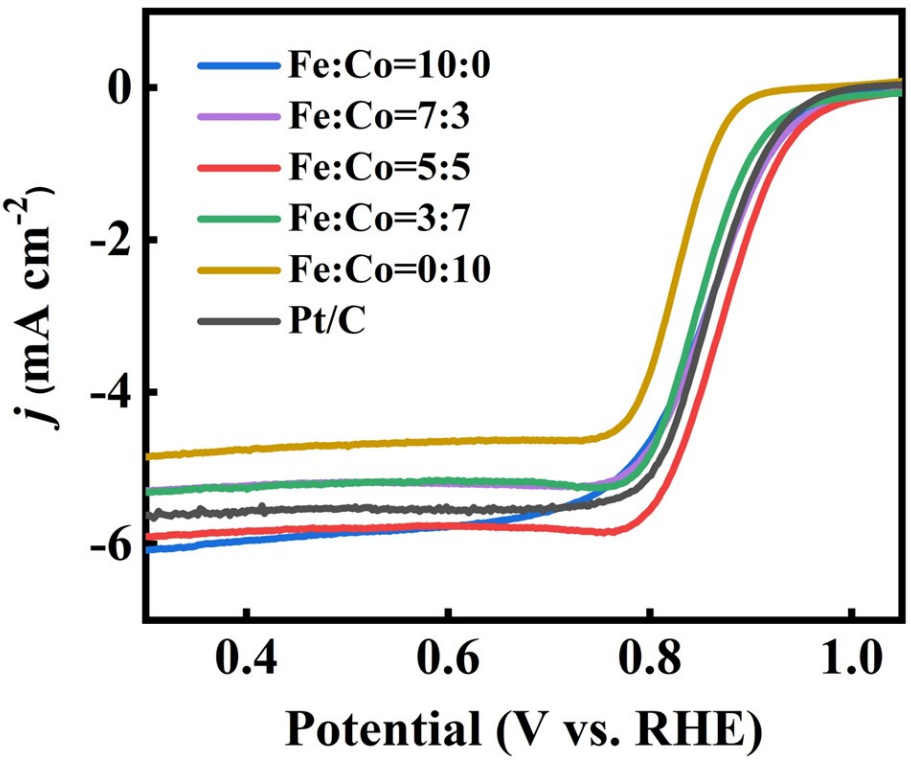

Figure S10. LSV comparison of between FeCo@PCNFs and control samples with different Fe/Co ratios in O_2-saturated 0.1M KOH solution at a sweep rate of 5 mV^{-1} and electrode rotation speed of 1600 rpm.

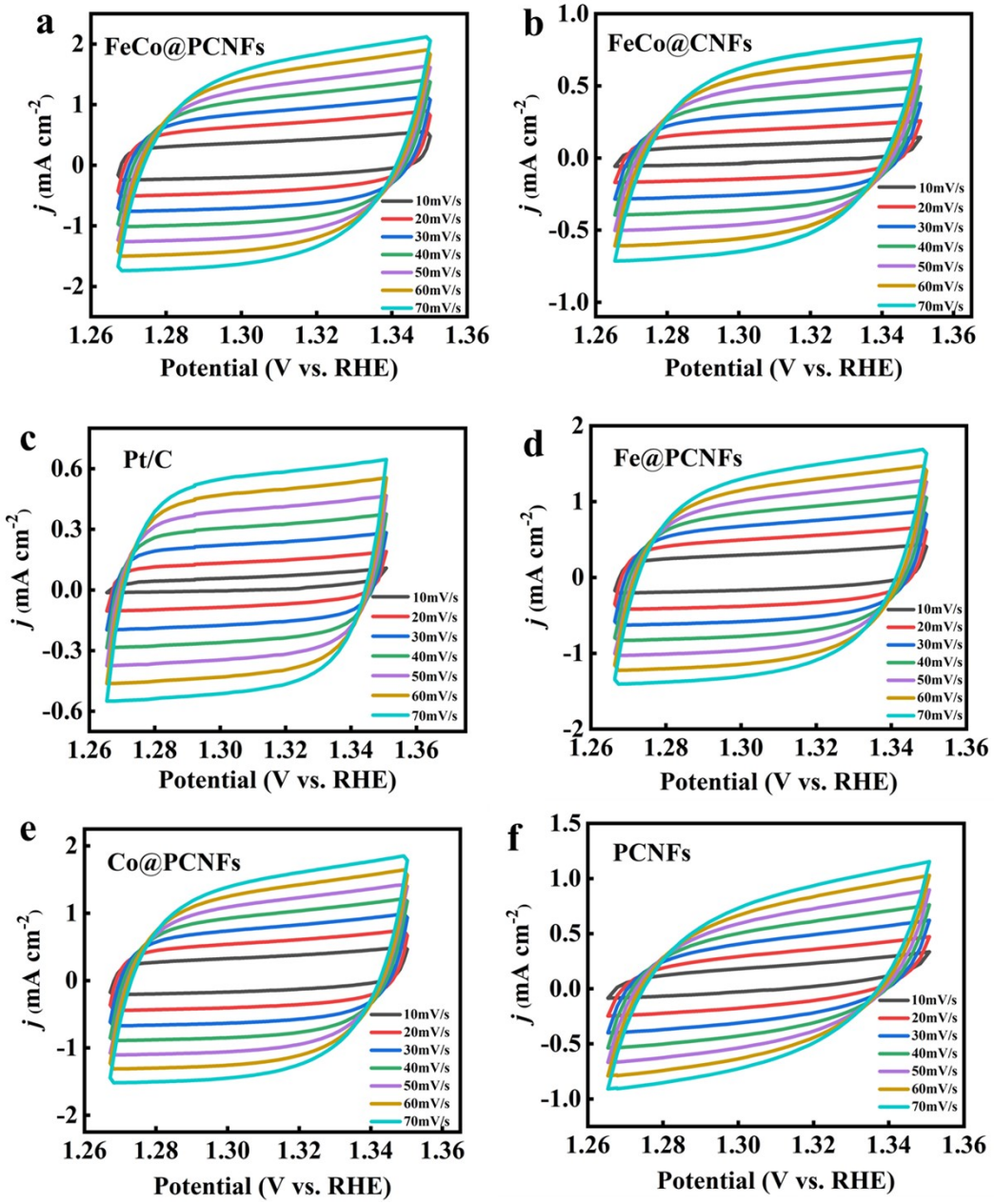

Figure S11. CV curves within a potential window from 1.267 to 1.350 V vs. RHE without Faradaic processes at various scan rates of 10, 20, 30, 40, 50, 60, and 70 mV s^{-1}. (a) Fe@PCNFs; (b) Co@PCNFs; (c) FeCo@PCNFs; (d) Pt/C; (e) Fe@PCNFs; (f) FeCo@PCNFs.

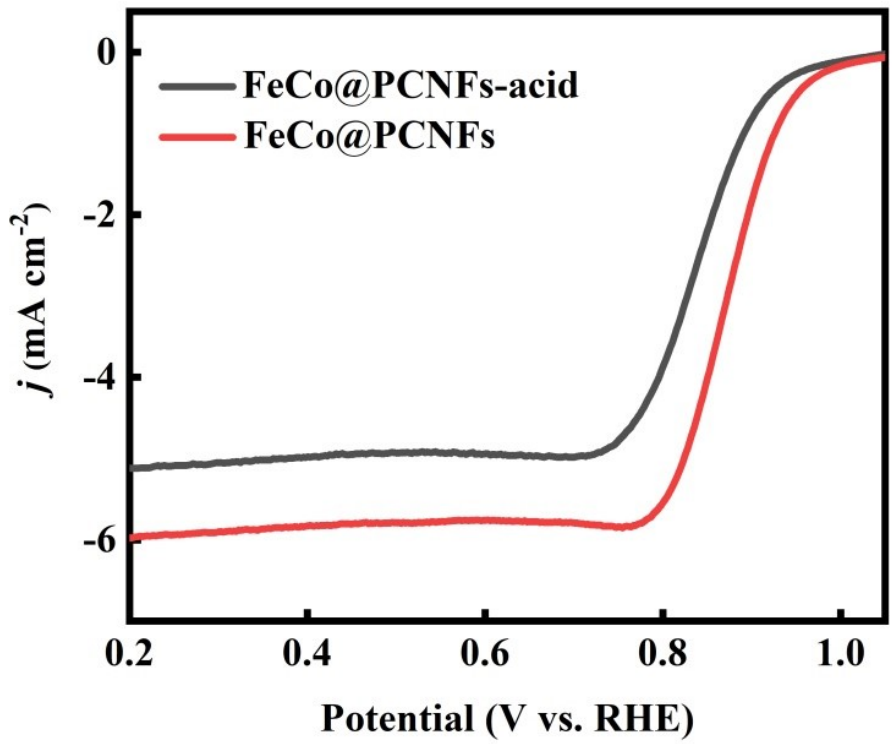

Figure S12. LSV comparison of FeCo@PCNFs and FeCo@PCNFs-acid in O_2-saturated 0.1M KOH solution at a sweep rate of 5 mV^{-1} and electrode rotation speed of 1600 rpm.

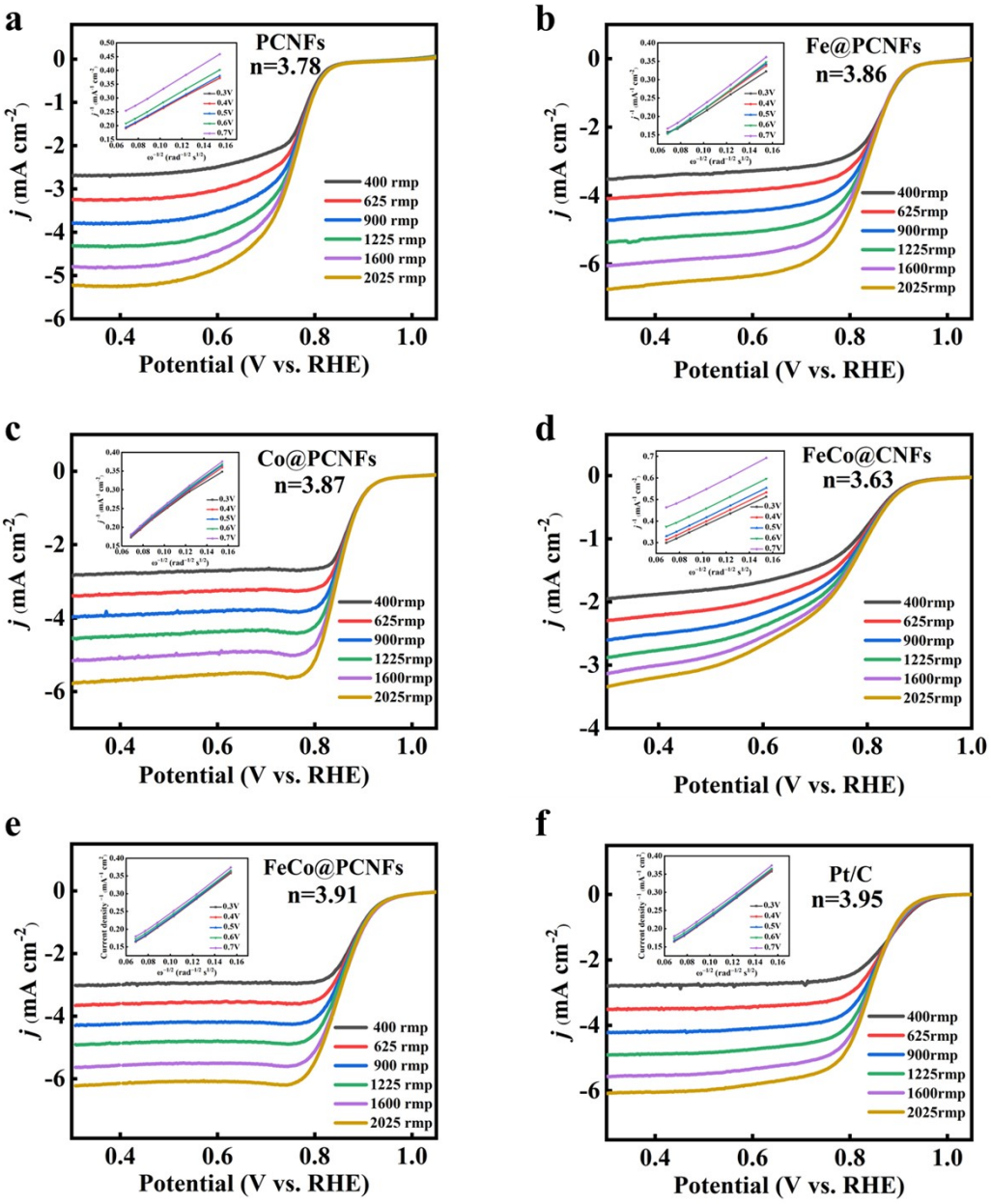

Figure S13. RDE polarization curves of different electrocatalysts at different rotating speeds, and the inset shows corresponding K−L plots at different potentials and electron transfer number.

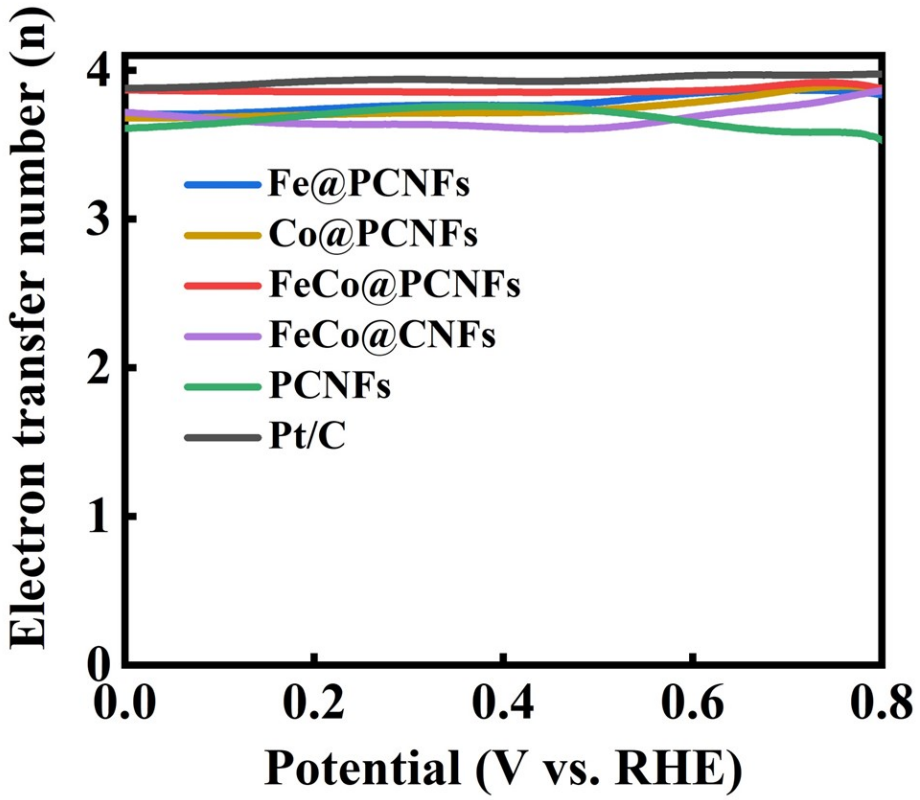

Figure S14. Electron transfer number of all samples calculated from RRDE data.

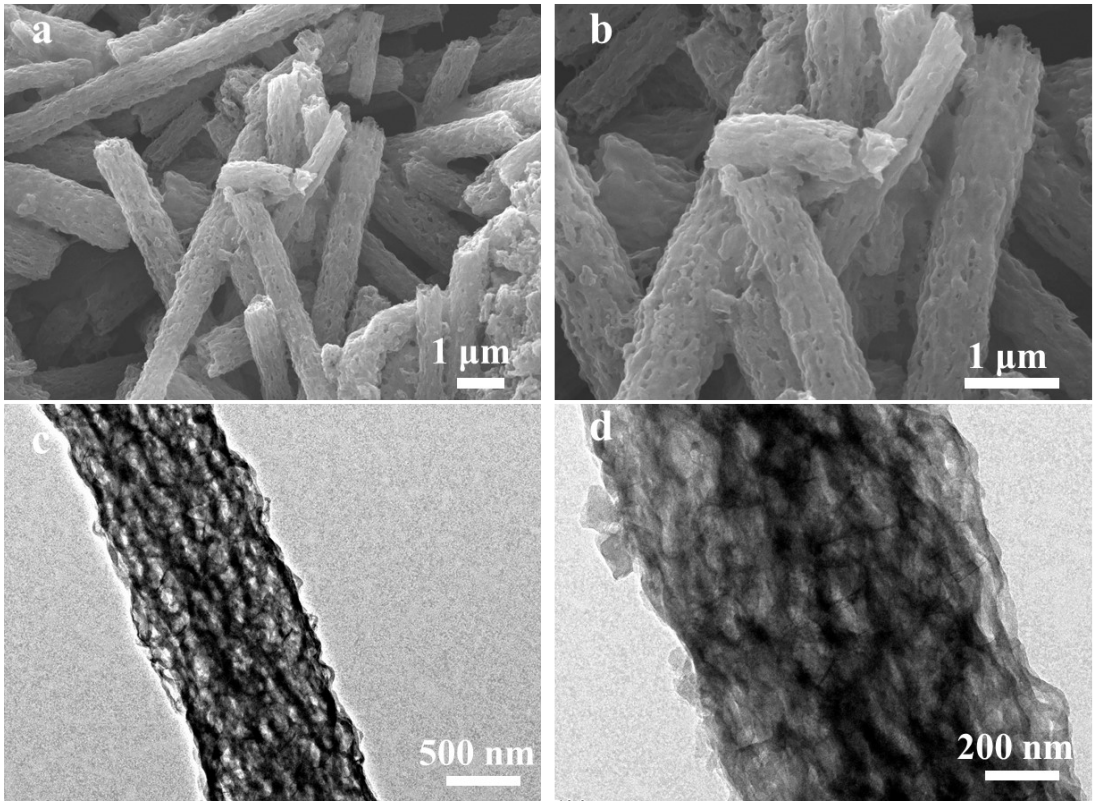

Figure S15. SEM and HRTEM images of FeCo@PCNFs after 32 h chronoamperometric curve.

Table S1. BET surface area, pore volumes and EDLC values for all samples.

Samples	BET surface area (m^2 g^{-1})	BJH Adsorption average pore diameter (nm)	BJH Adsorption cumulative volume of pore(cm^3 g^{-1})	EDLC (mF cm^{-2})
FeCo@PCNFs	481.76	22.19	0.69	22.3
FeCo@CNFs	302.70	5.24	0.22	9.7
Fe@PCNFs	444.29	17.79	0.39	18.1
Co@PCNFs	438.68	19.02	0.64	19.8
PCNFs	220.03	21.7	0.61	6.4
Pt/C	/	/	/	8.4

Table S2. The integral areas values of D and G peaks of obtained samples measured from Raman results.

Samples	A_D	A_G	I_D/I_G
PCNFs	276480.41	99216.38	2.79
Fe@PCNFs	277058.74	103514.30	2.68
Co@PCNFs	201095.72	80440.48	2.49
FeCo@CNFs	268580.58	159080.68	1.69
FeCo@PCNFs	194345.52	74617.56	2.60

Table S3. ICP-OES results of Fe and Co elements in different catalysts.

Samples	Fe	Co
FeCo@PCNFs	0.84%	0.83%
FeCo@CNFs	2.21%	2.58%
Fe@PCNFs	1.58%	/
Co@PCNFs	/	1.93%

Table S4. Surface atomic content of all samples obtained from XPS.

Samples	(Atomic ratio %)				
	C	N	O	Fe	Co
FeCo@PCNFs	88.61	3.65	6.75	0.53	0.46
Fe@PCNFs	82.38	7.99	8.76	0.88	/
Co@PCNFs	84.1	7.99	6.9	/	1.01
PCNFs	81.74	11.4	6.86	/	/

Table S5. Information of N content for different samples from XPS results.

Samples	Relative peak area percentage (%)			
	Pyridinic-N	**Pyrrolic-N**	**Graphitic-N**	**Oxidized -N**
FeCo@PCNFs	21.53	24.79	48.77	4.91
Fe@PCNFs	40.68	24.40	18.89	16.03
Co@PCNFs	31.16	22.28	30.04	16.52
PCNFs	42.98	22.81	21.05	13.16

Table S6. Comparison of ORR performance between FeCo@PCNFs and other reported Fe-, Co-based electrocatalysts under O_2-saturated 0.1 M KOH.

Catalyst	Loading (mg cm^{-2})	E_{onset} (V_{RHE})	$E_{1/2}$ (V_{RHE})	Reference
NiCoP/CNF900	0.5	/	0.82	*Adv. Energy. Mater.* **2018**, *8*, 1800555
Co@CNF-700	0.285	0.923	0.796	*J. Power Sources* **2018**, *380*, 174
FeCo-NCNFs-800	0.255	0.907	0.817	*ACS Sustainable Chem. Eng.* **2019**, 7, 5462
FeCo/Co_2P@NPCF	0.28	0.85	0.79	*Adv. Energy. Mater.* **2020**, *10*, 1903854
Fe_3C@MHNFS	0.2	/	0.90	*J. Mater. Chem. A* **2020**, *8*, 18125
FeCo-NC	0.1	0.981	0.848	*Chem. Eng. J.* **2020**, *395*, 125158
CoFe@HNSs	0.24	0.998	0.897	*Chem. Commun.* **2021**, *57*, 2049
FeCo/Se-CNT	/	0.97	0.9	*Nano Lett.* **2021**, *21*, 2255
Fe_1Co_1-CNF	0.2	0.99	0.87	*Nano Energy* **2021**, *87*, 106147
FeCo-N-HCN	0.1	0.98	0.86	*Adv. Funct. Mater.* **2021**, *31*, 2011289
NPC/FeCo@NCNT	0.2	0.92	0.835	*Adv. Sci.* **2021**, *8*, 2004572
Pd/FeCo	0.42	0.98	0.85	*Adv. Energy Mater.* **2021**, *11*, 2002204
Fe_1Co_3−NC-1100	0.736	1.05	0.877	*ACS Catal.* **2022**, *12*, 1216
FeCo@PCNFs	0.5	0.97	0.875	**This work**

Table S7. Summary of ORR performance for all samples in. Rotating disk electrode (RDE) results in terms of onset potential (E_{onset}) at 0.3 mA cm^{-2}, limiting current density (J_L), half-wave potential ($E_{1/2}$), kinetic current density (J_k) at 0.82 V and electron transfer number *n* under O_2-saturated 0.1 M KOH.

Catalyst	E_{onset} (V_{RHE})	$E_{1/2}$ (V_{RHE})	J_L (mA cm^{-2})	J_k at 0.82 V (mA cm^{-2})	Tafel slopes (mA dec^{-1})	*n*
Pt/C	0.94	0.86	5.6	26.6	111.7	3.92
FeCo@PCNFs	0.97	0.88	5.8	39.7	89.6	3.88
FeCo@CNFs	0.87	0.80	2.5	1.2	206.9	3.72
Fe@PCNFs	0.95	0.86	5.7	15.3	90.6	3.86
Co@PCNFs	0.88	0.83	4.7	7.0	111.1	3.82
PCNFs	0.81	0.73	3.7	0.2	135.6	3.61

Table S8. Compared with recently reported Fe-, Co-based electrocatalysts regarding the performance of Zn-Air batteries.

Catalyst	Loading (mg cm^{-2})	Open circuit potential (V)	Peak power density (mW cm^{-2})	Specific capacity (mAh g_{Zn}^{-1})	Reference
Co/Co-N-C	/	1.41	132	/	*Adv. Mater.* **2019**, *31*, 1901666
VC-MOF-Fe	1	1.49	113	/	*Nano Energy* **2020**, *82*, 105714
Co-NC-800	1	1.44	109.5	657.2 at 20mA^{-2}	*Chem. Eng. J.* **2020**, *409*, 128171
Co@hNCTs-800	2	1.45	149	746 at 10mA^{-2}	*Nano Energy* **2020**, *71*, 104592
Co/CNWs/CNFs	/	1.46	304	762 at 10mA^{-2}	*Adv. Funct. Mater.* **2021**, *31*, 2105021
A-Fe-NC	2	1.45	132.2	/	*Chem. Eng. J.* **2021**, *426*, 127345
Fe-doped MOF CoV@CoO	1	1.45	138	/	*Nano Energy* **2021**, *88*, 106238
0.05CoO_x@PNC	2	1.49	157.1	887 at 10mA^{-2}	*Nano Energy* **2021**, *83*, 105813
Co_2Cu_1–S	1	/	195	815.3 at 5mA^{-2}	*J. Mater. Chem. A* **2021**, *9*, 18329
Fe/SNCFs-NH_3	0.5	/	255.84	/	*Adv. Mater.* **2021**, *34*, 2105410
Co-N-CCNFMs/CC	1	1.497	90.3	/	*Energy Storage Mater.* **2022**, *47*, 365
SA&NP-FeCo-NTS	1.2	1.48	102.2	770.8 at 10mA^{-2}	*Adv. Funct. Mater.* **2022**, *32*, 2112805
Co@Fe-Nx/C	2	1.44	249	802 at 10mA^{-2}	*Chem. Eng. J.* **2022**, *436*, 135191
FeCo@PCNFs	2	1.48	289.5	764.5 at 10mA^{-2}	**This work**